INFLUENCE OF DCCSS BEARINGS OVER-STROKE AND BREAKAWAY ON THE SEISMIC RESPONSE OF ISOLATED BUILDINGS

F. C. Ponzo[1], A. Di Cesare[2], A. Telesca[3], D. Nigro[4], M. G. Castellano[5], S. Infanti[6]

[1] *Prof, School of Engineering, University of Basilicata, felice.ponzo@unibas.it*
[2] *Prof, School of Engineering, University of Basilicata, antonio.dicesare@unibas.it*
[3] *Dr, School of Engineering, University of Basilicata, alessio.telesca@unibas.it*
[4] *Dr, School of Engineering, University of Basilicata, domenico.nigro@unibas.it*
[5] *Dr, FIP mec srl, gabriella.castellano@fipmec.it*
[6] *Dr, FIP mec srl, samuele.infanti@fipmec.it*

Abstract

The underlying concept of base isolation is the uncoupling of the horizontal building movement from ground motions using a flexible isolation layer made with either elastomeric or sliding bearings. Double Concave Curved Surface Sliders *DCCSS* are seismic isolators based on the pendulum principle.

This paper focuses on the effects of the breakaway friction and of the over-stroke displacement capacity of *DCCSS* on the seismic response of base isolated buildings at different limit states. At the serviceability limit state, the breakaway friction is characterized by a peak in the friction coefficient at the start of motion that can prevent the proper sliding of devices resulting in stronger stresses on the superstructure. For the widely used in Europe isolators that do not include any mechanical elements that serve as end-stroke beyond their geometric displacement capacity (over-stroke regime), the inner slider runs on the edge of the sliding surfaces preserving the ability to support gravity loads for earthquakes stronger than the ultimate limit state ones.

The effects of the aforementioned DCCSS features on isolated structures have been analyzed considering a simple case study composed of a 2D moment resistant steel frame with 3 bays and 6 story representative of a residential use building, designed according to the Italian seismic code for high seismicity zone. Nonlinear static and dynamic analyses including inelastic superstructure and four basic model types for the DCCSS bearing behavior, with and without breakaway and over-stroke effects and with and without end stops, have been performed. The numerical model of the over-stroke effects has been calibrated on the results of a displacement-controlled test conducted by *FIP mec srl*. The numerical results have been compared in order to assess the influence of the DCCSS models on the seismic behavior of the superstructure and of the isolators designed conforming to European or other international codes. The research aims to identify critical aspects of the DCCSS isolators and to provide the basis for the subsequent computations about the probability of exceeding the superstructure yielding limit or reaching the isolators maximum displacement.

Keywords: Base isolation, Double concave curved surface sliders, Breakaway friction, Over-stroke displacement, Nonlinear analysis

1. Introduction

Base isolation is one of the most widespread techniques currently used for seismic protection of buildings and their equipment. At the ultimate limit state, the isolating devices are designed to attain the design displacement at the Maximum Considered Earthquake (MCE), while the superstructure remains in the elastic range at the Design Basis Earthquake (DBE) [1] [2]. Recent earthquakes demonstrated that correctly designed base isolated buildings can be used immediately even after strong earthquakes with no loss of building functionality [3].

Curved Surface Slider (CSS) bearing, as per definition of the European Standard on Anti-seismic devices [4], is one of the most widely used isolators for both buildings and bridges. Combining two sliding concave surfaces the resulting is the Double Concave Curved Surface Slider (DCCSS) bearing (Fig. 1), which produces two independent pendulum response mechanisms and can be modeled as a series of two CSSs. In case of equal radius of curvature and same coefficient of friction on the upper and lower surfaces, sliding occurs simultaneously on both surfaces until extreme conditions such as uplift and/or contact with the displacement restraints are reached. The effectiveness of isolation systems based on curved surface sliders has been proven by experimental campaigns and analytical studies [5][6][7][8][9] investigating on main aspects such as the influence on the friction coefficient of vertical load, of velocity of motion and of frictional heating and on the re-centring capability of the system.

Recent studies consider the isolation system failure that may occur when the movement in the sliding surfaces produces vibrations to the superstructure, such as those induced by the breakaway phenomenon [10], or when the actual isolator displacement capacity d_C is exceeded, see Fig. 1(a), such as when earthquakes stronger than the design one happen [11] [12]. The Breakaway effect consists of a sudden coefficient of friction increase at the beginning of the motion, regardless of the axial load and the sliding velocity, that can cause peaks of acceleration on the superstructure under low seismic motions. The use of end-stroke restraints (end stops) such as restraining rings showed in Fig. 1(a) is admitted by American standard [13] [14]. On the contrary, the European Standard [4] does not allow the presence of an end-stroke but consents the use of joints separating the superstructure from the surrounding ground or construction walls, see Fig. 1(b), larger than the maximum displacement capacity of the isolators, in order to safely accommodate the seismic movement. In this case, the inner slider could run on the edge of the sliding surfaces in the over-stroke regime, preserving the ability to support gravity loads and the re-centring capability.
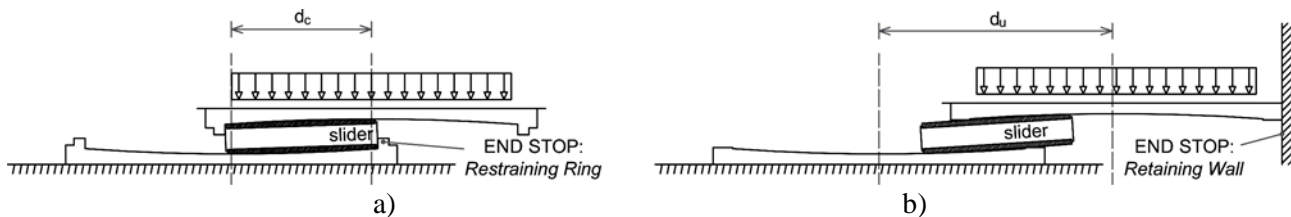

Fig. 1 – Maximum lateral displacement of DCCSS Isolators: a) with restraining ring dc; b) with overstroke capacity and retaining wall du

Fig. 2 shows the results of experimental tests performed by *FIP MEC srl* [15] on DCCSS beyond the geometric displacement capacity of isolator Fig. 1(b) applying constant vertical load (2500kN) and low velocity (2.5mm/s). Experimental results show that at the first cycle, the load-bearing capacity of the device is not compromised until the slider overcomes the concave sliding surfaces edge up to a quarter or half of sliding pad diameter, resulting in a slight increase of stiffness and friction coefficient. The test shows a breakaway friction condition in the first loading branch, see Fig. 2(a), due to the very slow velocity applied during the test in order to provide good control of vertical loading instability. Both in loading and unloading phases, the DCCSS over-stroke cyclic behaviour is characterized by a "sloping dog bone" shape.
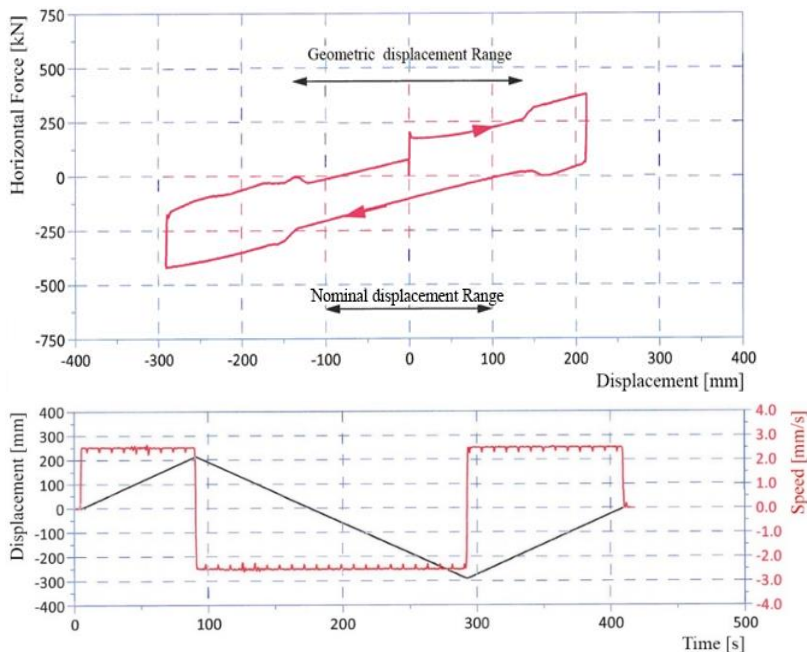
2

Fig. 2 – Results of experimental test on DCCSS Isolator with over-stroke displacement.

2. Case study

This study is based on a 6-story residential building, classified as ordinary thus the importance factor is $c_u = 1$, considered as case study in various research papers [7] [11] [12] or guidelines [16] [17] and codes [13]. The moment resistant steel frame elevations and the cross-sections of structural elements are shown in Fig. 3(a). The isolated building shown in Fig. 3(b) is designed according to the Italian seismic code [2] for a location in the city of L'Aquila, central Italy, and medium soil class C, see Fig. 4(a). The bare frame has been designed for gravity loads only respecting minimum criteria required by Eurocode [1] while considering low ductility class for structural details. The seismic weights W_i and masses M_i of each floor, see Fig. 3(b), are listed in Table 1. The total seismic weight W of the isolated frame is about 5000kN and the vertical load on the internal isolators is $N_{Sd} = 1680$kN.
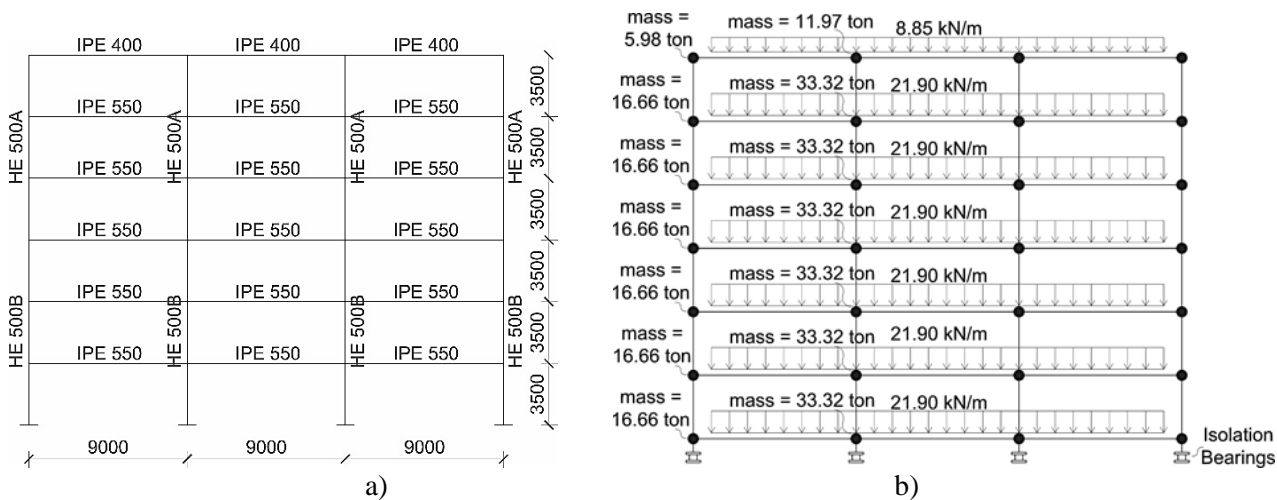

Fig. 3 – a) Structural elements of the fixed-base superstructure; b) Representation of gravity loads for moment resisting frame of isolated building.

3

Table 1 – Structural elements sections and seismic loads and masses of the prototype frame.

Floor	Structural load G_1 [kN/m]	Permanent load G_2 [kN/m]	Variable action Q [kN/m]	Weighs W_i [kN]	Masses M_i [ton]
Base	8	8.5	18	970	99
1st, 2nd and 3rd	8	8.5	18	980	100
4th and 5th	8	8.5	18	980	100
6th	4	3.5	4.5	350	36

2.1 Design of isolation system

The isolation system consists of four DCCSS isolators placed below each column. The behavior of the DCCSS with equivalent radius R_e and friction coefficient μ of both sliding surfaces becomes equal to that of a CSS shown in Fig. 4(b). The isolators are based on the pendulum mechanism, that generates the restoring force, the restoring stiffness K_p, and the friction force F_0. Following Eq. (1), the equivalent restoring stiffness k_p and the friction force F_0 are function of the equivalent radius R_e, the vertical load N_{sd} and the friction coefficient μ.

$$F_0 = \mu\, N_{sd} ; \qquad\qquad k_p = \frac{N_{sd}}{R_e} \tag{1}$$

The effective period T_e of the isolated structure becomes independent from the mass of the superstructure M, as it only depends on the equivalent radius R_e. The pre-sliding stage of motion has been modelled by a quasi-rigid behavior with initial stiffness k_i. The design displacement d_{Ed} of the isolation system is obtained considering the MCE reduced by the effective damping ξ_{eff}, see Eq. (2). Considering the industrial discretization of geometrical dimensions and the commonly used sliding materials, in line with the currently available values of commercial bearings, a maximum displacement capacity $d_C = 300$mm and a vertical load capacity $N_{Ed} = 2000$kN of the isolators are assumed. Considering the limited experimental data available about the actual displacement capacity of double curved surface devices, an over-stroke ultimate displacement d_U equal to 1.5 $d_C = 450$mm has been conservatively assumed. Main design parameters of the isolation system are reported in Table 2.

$$K_e = N_{Sd} \cdot \left(\frac{1}{R_e} + \frac{\mu}{d_{Ed}}\right); \qquad \xi_{eff} = \frac{2}{\pi} \cdot \frac{1}{\left(\frac{d_{Ed}}{\mu \cdot R_e}\right)+1} ; \qquad T_e = 2\pi \sqrt{\frac{1}{g \cdot \left(\frac{1}{R_e}+\frac{\mu}{d_{Ed}}\right)}} \tag{2}$$
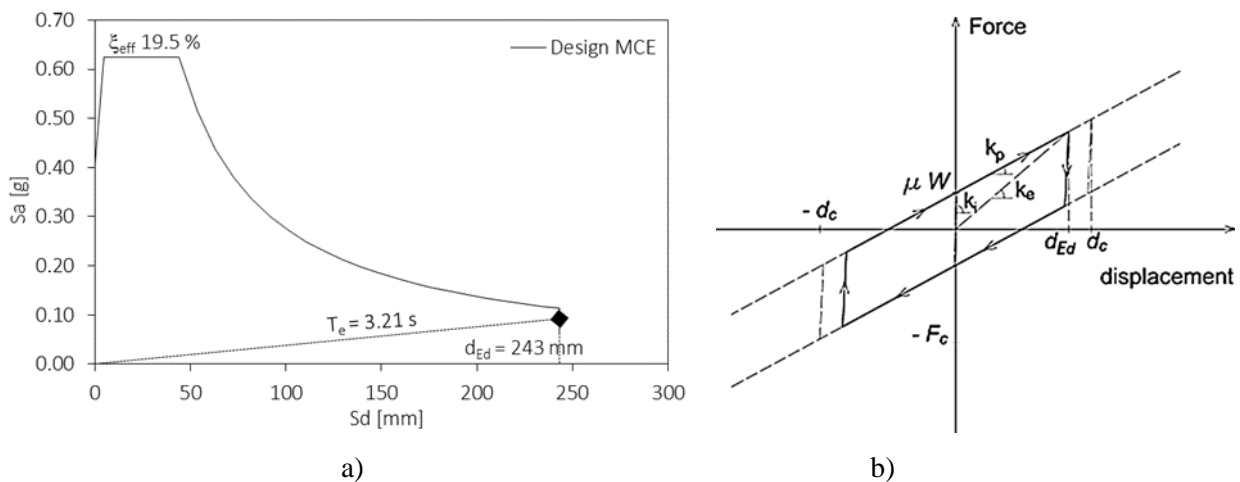

Fig. 4 – a) Design of isolation system, b) force-displacement relationship of DCSS isolators

4

Table 2 – Isolation system design parameters.

R_e [mm]	N_{sd} [kN]	N_{Ed} [kN]	μ [%]	K_i [kN/m]	K_e [kN/m]	T_e [sec]	ξ_{eff} [%]	d_{Ed} [mm]	d_c [mm]	d_u mm
3700	1680	2000	2.9	5000	653.15	3.21	19.5	243	300	450

2.2 Numerical model

A nonlinear numerical model including both inelastic superstructure and isolation devices is adopted by using OpenSEES [18] [19]. In particular, accurate nonlinear models have been developed for the isolation devices in order to correctly predict the over-stroke response of the isolated building.

A lumped plasticity model has been considered for beam and column elements of the superstructure, whereas elastic beams have been used for the base floor grid above the isolation system. Plastic hinges have been concentrated at the end of structural elements at distance from end nodes equal to the element depth. Panel zones were modeled with rigid elastic elements by using a two-nodes link element with length equal to half the section depth, Fig. 5(a). Member capacities were calculated using the expected yield strength of the steel material 275 MPa.

Four basic model types for the DCCSS bearing behavior, with and without breakaway and over-stroke effects and with and without end stops, see Fig. 5(b), have been considered. In particular, the isolation system configurations considered were: i) basic isolation model (BI) with unlimited elasto-plastic behavior; ii) BI with end-stroke d_{max} = 300mm; iii) BI with breakaway and unlimited over-stroke; iv) BI with breakaway and over-stroke with end-over-stroke $d_{max.}$ = 450mm.
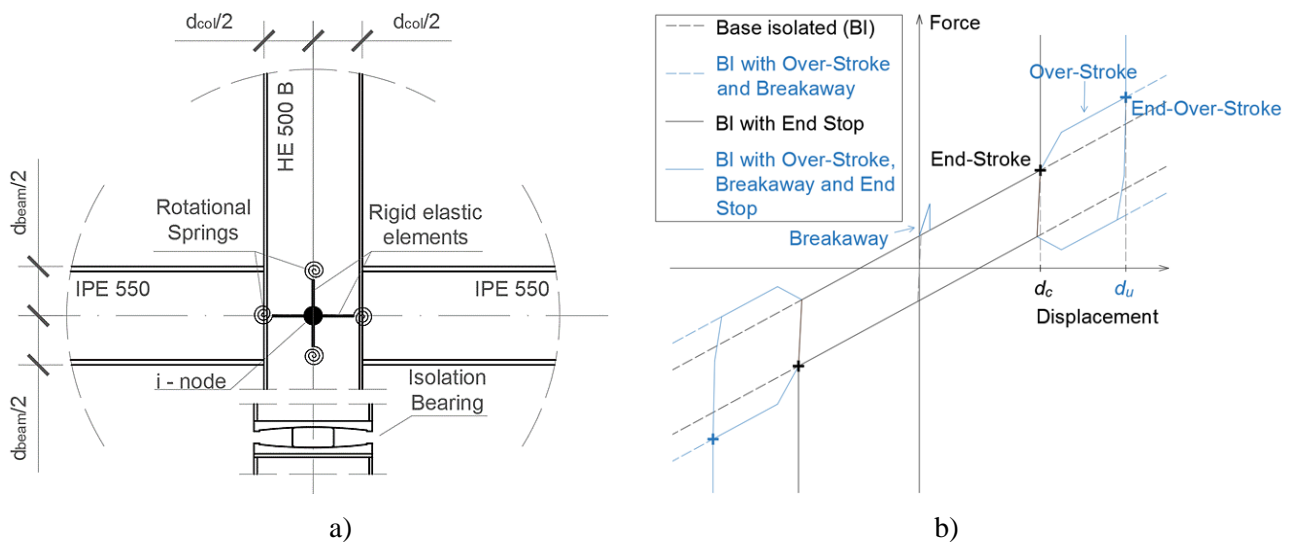

Fig. 5 – a) Model of beam-column joints of the superstructure. b) model of force-displacement behavior of four isolation systems considered in this study.

For the basic model of Base Isolation (BI), the Single FP Bearing element implemented in OpenSEES has been selected to describe the cyclic behaviour of the basic DCCSS isolator shown in Fig. 4(b), zero-length sliding hinge from i-node to j-node of Fig. 6(a). The friction coefficient is modelled accounting for its dependency on sliding velocity [20], while the effects of temperature and contact pressure are neglected. The values of the mechanical properties of DCCSS listed in Table 2.

Seismic stoppers consisting of a zero-length gap element with infinitely rigid behavior were added to the basic model of each isolator [22] from i-node to s-node of Fig. 6(a). The model is not dissipative during

5

the impact between the rigid retaining (restraining ring or moat wall) and the sliding pad or the base slab. The gap amplitude d_{max} was assumed equal to the displacement capacity of the bearings d_C for the analysis of BI, see Fig. 5 and Table 2, and to the ultimate displacement d_U for the case of BI with over-stroke, see Fig. 6(b) and Table 3.

In order to simulate the behavior of DCCSS bearing during the over stroke displacement, the numerical model has been modified by adding three zero-length parallel hinges to the basic model of BI from *j*-node to *k*-node, as shown in Fig. 6(a) [23]. Two elastic-perfectly plastic gap elements shown in Fig. 6(d) are defined by a gap displacement d_C, elastic stiffness k_2 and increased friction coefficient $\Delta\mu$ with no hardening ratio or damage accumulation are considered. One multi-linear elastic element, characterized by a nonlinear elastic behavior without energy dissipation, is defined by a set of stress-strain points, as shown in Fig. 6(e). The elements parameters defined for the case study are listed in Table 3. The force-displacement behavior of the modified DCCSS model is shown in Fig. 6(f).
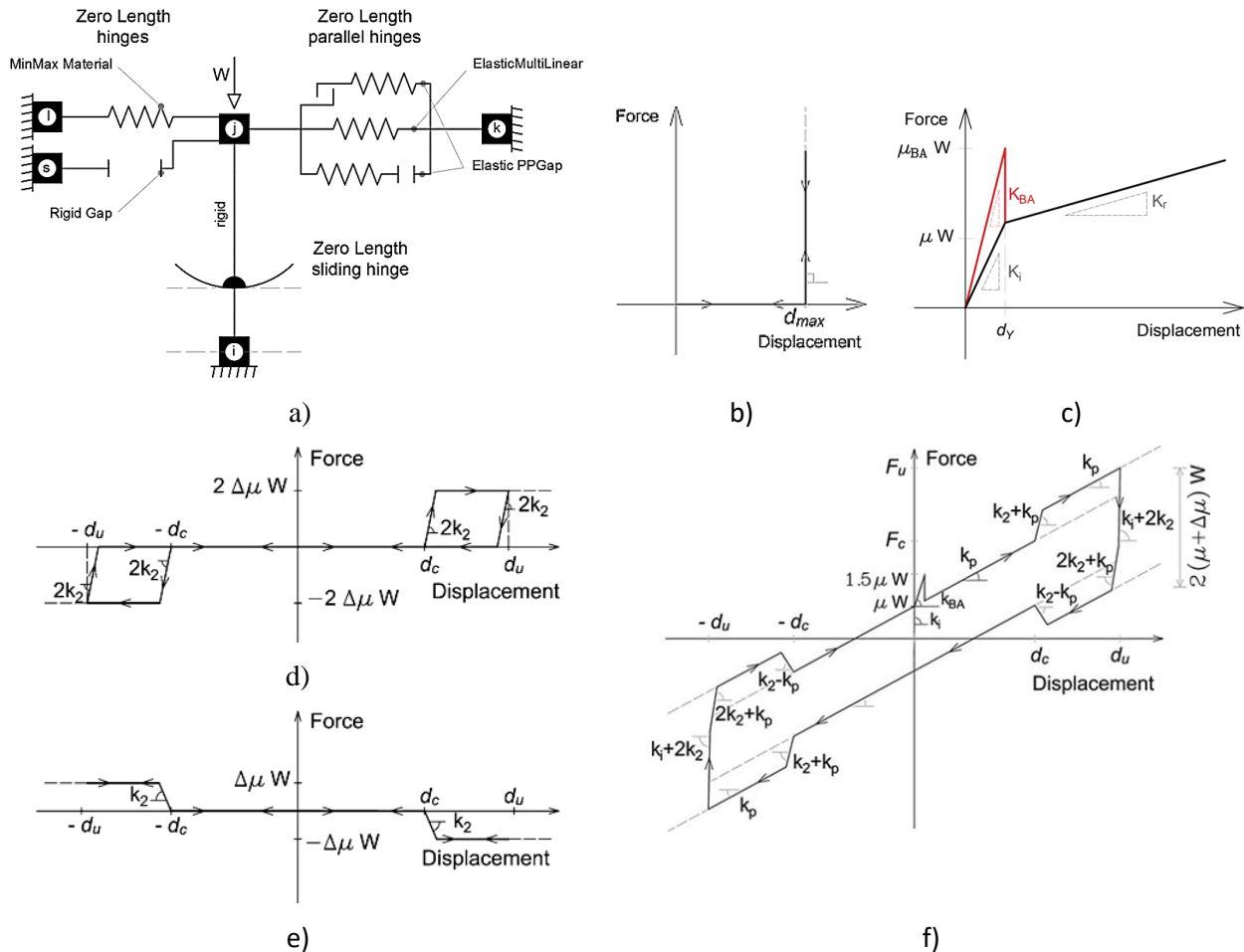

Fig. 6 – (a) Modified model of OpenSEES CSS Bearing; (b) compression gap model considered for the seismic stopper; (c) constitutive law representing the Breakaway effect; (d) elasticPPGap materials and (e) elastic multi-linear material for the over-sroke displacement, (f) composed model.

The Breakaway effect was modeled by introducing a zero-length min/max hinge from *j*-node to *l*-node as shown in Fig. 6(a). When the element strain falls above the initial elastic displacement d_y it is excluded from the analysis. The breakaway force F_{BA} depends on the breakaway stiffness k_{BA} and on the breakaway friction coefficient μ_{BA} as reported in Fig. 6(c). The Breakaway coefficient of friction value has been derived from available literature [21] and from the database of several experimental tests performed on full-size double and

6

single curvature bearings carried out according to Eurocode provisions [4] at *SisLab* of the University of Basilicata *(www.unibassislab.it)*. It has been set as 1.5 times the value of friction coefficient $\mu_{BA} = 1.5 \ \mu$.

Table 3 – Isolation system model parameters.

End-stop model	Over-Stroke model			Breakaway model	
d_{max} mm	k_2 kN/mm	$\Delta\mu$ -	μ_2 -	k_{BA} kN/mm	μ_{BA} -
300 or 450	2.50	0.02	0.06	3.28	0.06

3. Analyses and results

Non-linear static analyses were carried out as described in [14] [17]. The pushover analysis of four cases of isolation systems and of a non-isolated frame are presented in Fig. 7. A distribution of lateral force proportional to the floor masses was used in the analysis. The graphs indicate the point (cross) where isolators reach the end stops. The pushover curves are shown beyond the isolator end-stroke point (in dashed line) to denote the behavior when isolators of unlimited ultimate displacement are assumed. A square in the pushover curves shows the point where the maximum story drift ratio reached the limit of 1%, which is the design drift of the isolated frame. From the pushover curves may be observed that the exceedance of the maximum displacement of the isolators occurs prior to the design drift when the superstructure starts yielding. Moreover, while the shape of the curve for the non-isolated structure can be reasonably approximated by an elastoplastic representation, the pushover curves of the isolated structures cannot. This means that pushover curves could not be always used in the application of the simplified procedure for spectral shape effect estimation. The behavior without end stops (dashed line) and with end stops placed at distance d_{max} demonstrate that the location of retaining elements should be consistent with the superstructure strength. The pushover curves of case studies without end stops highlight that the design drift occurs due to excessive deformations in the superstructure and it is linked to excessive displacement of the isolators.
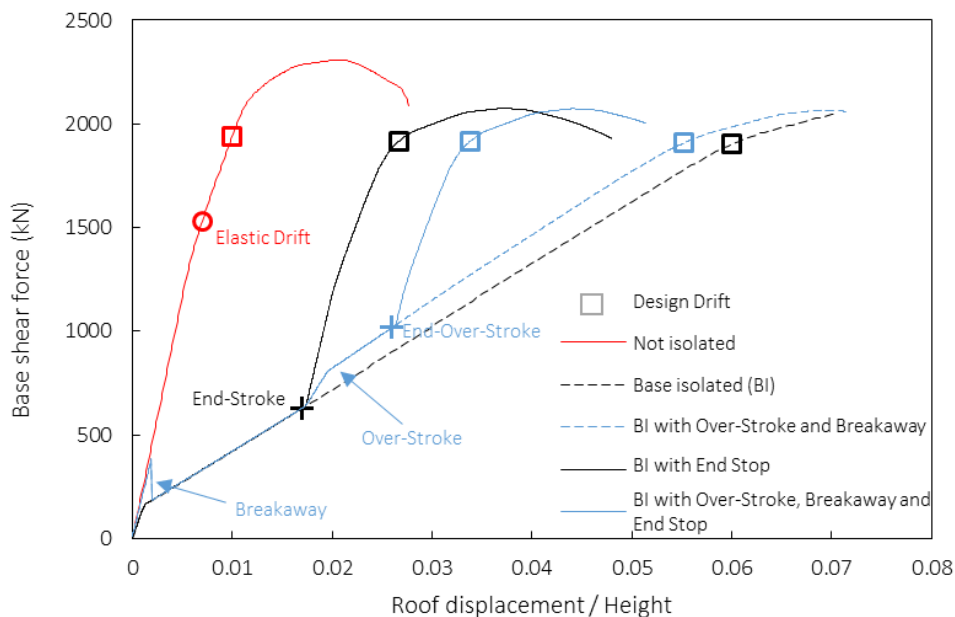

Fig. 7 – Pushover curves of fixed base model and of four cases of isolation systems.

The relation between structural and isolator limits obtained from pushover analyses has been confirmed through inelastic response history analyses of seismically isolated structures. Multi-Stripe nonlinear time history analyses have been carried out considering 10 intensity levels with 20 ground motions per each intensity. In particular, the Intensity Measure (IM) selected to represent the earthquake intensity levels is the spectral acceleration (5%-damped) corresponding to a reference period (conditioning period) chosen as close as possible to the design value of the fundamental period of vibration of the base-isolated building (T = 3 sec). The compatibility with a Conditional Mean Spectrum (CMS) assures that all the selected records are scaled so that they have the same spectral ordinate at the conditioning period for each intensity levels. As an example, the elastic spectra of 20 seismic inputs of the intensity measure level IM6 corresponding to MCE [2] is reported in Fig. 8.

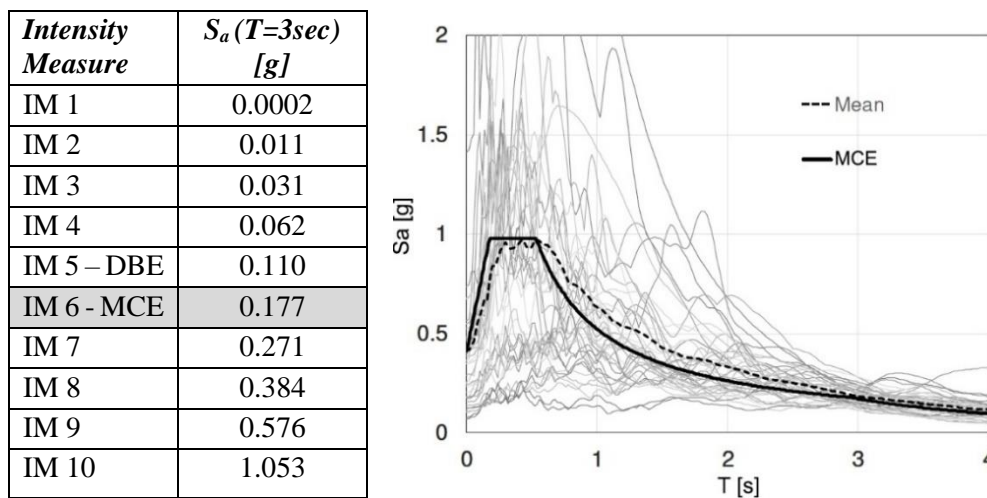| Intensity Measure	$S_a(T=3sec)$ [g]
IM 1	0.0002
IM 2	0.011
IM 3	0.031
IM 4	0.062
IM 5 – DBE	0.110
IM 6 - MCE	0.177
IM 7	0.271
IM 8	0.384
IM 9	0.576
IM 10	1.053

Fig. 8 – Ground motions selected for the multi-stripe analysis and elastic spectra of seismic inputs at IM 6.

The limit values of the engineering demand parameters (EDP) associated with base displacement and superstructure drift have been defined as summarized in Table 4. Sliders displacement limits are assumed equal to the displacement capacity d_C of the isolators in case of BI model or equal to the ultimate displacement d_u in case of BI with over-stroke model. The restraining ring failure due to the impact against the inner slider is not accounted for in this study. For the superstructure, a conventional drift limit equal to 1% has been adopted. In particular, this limit represents the condition for safety verifications of the structural elements at the ultimate limit state, taking into account a behavior factor of 1,5 from the lateral strength elastic limit on the fixed-base superstructure pushover.

Table 4 – Exceedance limit condition.

Component	EDP	Base isolated model	Limit value
Superstructure	Global Drift	all models	drift 1%
Isolation system	Isolator displacement	w/o over-stroke	d_{max} = 300 mm
		with over-stroke	d_{max} = 450 mm

Results of analyses carried out on the same case study building considering the presence of seismic stoppers and of over-stroke and breakaway effects are reported in Fig. 9 and Fig. 10.

In Fig. 9 are shown the fragility curves defined as the probability of reaching or exceeding the specified limit of EDPs under earthquake excitations. The fragility curves are established to provide a prediction of potential damage during an earthquake higher than the MCE (corresponding to IM6).

8

A lognormal cumulative distribution function Eq. (3) is often used to define a fragility function where $P(C|IM = x)$ is the probability that a ground motion with $IM = x$ will cause the structure to reach an EDP limit value; $\Phi(\ )$ is the standard normal cumulative distribution function (CDF); θ is the median of the fragility function (the IM level with 50% probability of exceeding); and β is the standard deviation of $\ln IM$ (sometimes referred to as the dispersion of IM) [25].

$$P(C|IM = x) = \Phi\left(\frac{\ln(x/\theta)}{\beta}\right) \tag{3}$$

Fig. 9(a) shows the fragility curves referred to the isolator displacement EDP for the cases of isolation systems with and without stoppers. It is observed that the BI with over-stroke model demonstrates better performances compared to the case with the restraining ring, resulting in a lower vulnerability level of the isolation system. In particular, the probability to impact against the displacement retaining at IM6 is about 15% for the case of BI model and about 5% for in case of BI with over-stroke model. This result is a direct consequence of the different isolator displacement limits assumed but is also due to the over-stroke effect that increases the damping of the isolation system. Fig. 9(b) shows the fragility for the superstructure drift that exceed 1% for all isolation system cases. For high-intensity ground motions levels, the presence of the isolator displacement retaining element has a strong influence on the performance of the superstructure. When the end stops are present, the over-stroke capacity increases the seismic performance of the superstructure.
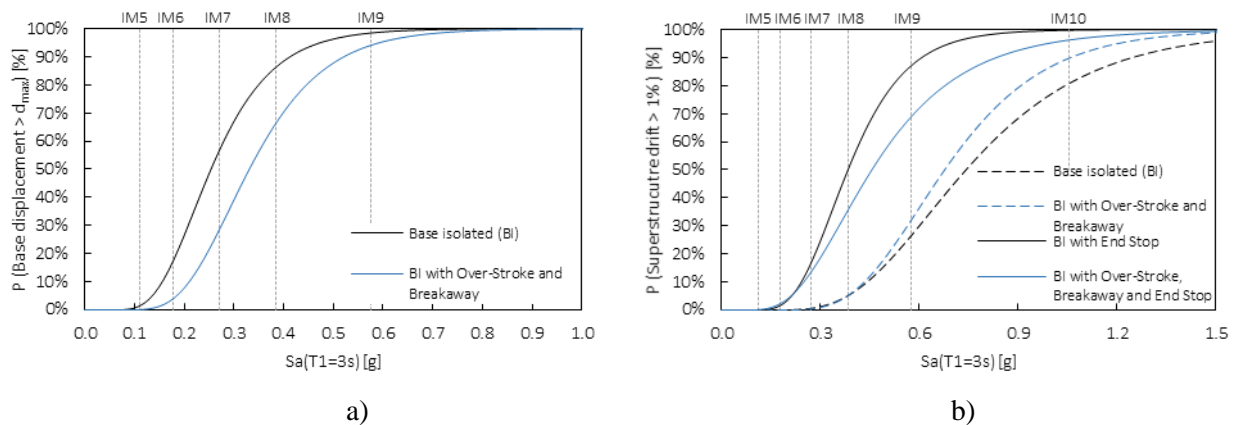

Fig. 9 – Fragility Curves as function of $Sa(T=3sec)$ representing the probability of exceeding: a) the isolator displacement limits d_{max}; b) the superstructure drift limit 1%.

The box-and-whisker (five-number summary) plots of Fig. 10 show the minimum, first quartile, median, third quartile, and maximum of the superstructure drift for all isolation systems. The box is bounded on the top by the third quartile, and on the bottom by the first quartile. The median divides the box. The whiskers are error bars: One extends upward from the third quartile to the maximum, and the other extends downward from the first quartile to the minimum.

For models without stoppers, Fig. 10(a), the drift limit is mainly exceeded when over-stroke is considered. Differently, for models with stoppers Fig. 10(b), the over-stroke capacity has no influence on the superstructure drift. The reason is that once the gap amplitude is reached, the acceleration resulting from the impact is immediately transferred to the superstructure. If the impact is strong, shear forces induced by such accelerations are large and can cause the collapse of the restraining ring. Looking at low seismic intensities, drift values are similar in cases of building with and without stoppers, while are higher when breakaway effects are considered.
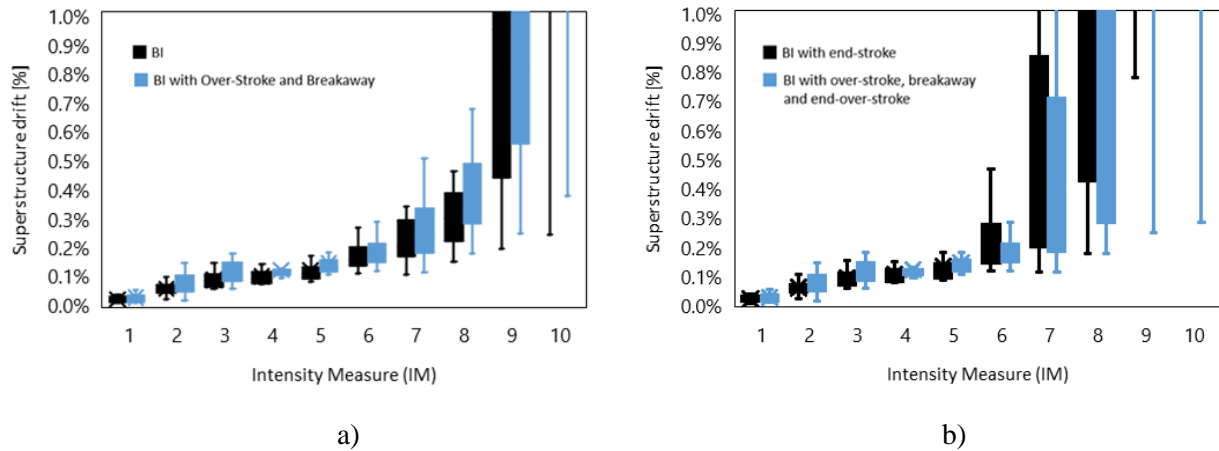
9

a)   b)

Fig. 10 – Superstructure global drift for the case: a) with seismic stoppers; b) without seismic stoppers

4. Considerations

Exposed results show how the displacement retaining (end stop) sets as a determining factor in the isolation system failure condition assessment and how the over-stroke effect can play as an additional safety factor for earthquakes strongest then Ultimate Limit State (ULS) considered for the design of isolation system. For high intensity levels of ground motion, the superstructure has shown a significant dependence on displacement restrainers, while the over-stroke and breakaway effects have no influence on the maximum drift. On the other hand, for low seismic intensities, the breakaway affects the superstructure seismic behavior.

The presented studies were limited to one case study of moment steel frame and are based on an experimental test on the over-stroke displacement of a double concave curved surface slider (DCCSS) without restraining ring. Therefore, further experimental tests and studies accounting for the failure of the restraining ring and considering also the top floor acceleration as engineering demand parameter to control the vibrations of the superstructure, considering also existing reinforced concrete buildings, are currently underway.

References

[1] EN 1998-1. Eurocode 8: Design of structures for earthquake resistance - Part 1: General rules, seismic actions and rules for buildings. European committee for standardization (CEN), Bruxelles, Belgium 2004.

[2] NTC 2018 "Italian Technical Code for constructions (in Italian)." Ministry of Infrastructures, Italy 17/01/2018.

[3] KAWASHIMA, K. "Damage of bridges due to the 2011 great east japan earthquake." Journal of Japan Association for Earthquake Engineering, 12(4), 2012, 319–338.

[4] UNI EN. "15129: Anti-seismic devices." European committee for standardization (CEN), Bruxelles, Belgium 2009.

[5] KUMAR, M., WHITTAKER, A.S., CONSTANTINOU, M.C. "Characterizing friction in sliding isolation bearings", Earthquake Engineering and Structural Dynamics, Vol. 44(9), pp. 1409– 1425, 2014.

[6] LOMIENTO, G., BONESSIO, N., BENZONI, G., "Friction Model for Sliding Bearings under Seismic Excitation", Journal of Earthquake Engineering, Vol. 17(8), pp. 1162-1191, DOI: 10.1080/13632469.2013.814611, 2013.

[7] MCVITTY WJ, CONSTANTINOU MC. "Property modification factors for seismic isolators: design guidance for buildings". Buffalo, NY: Multidisciplinary Center for Earthquake Engineering Research, 2015.

10

2g-0192

[8] PONZO, F. C., DI CESARE, A., LECCESE, G., & NIGRO, D. "Shake table testing on restoring capability of double concave friction pendulum seismic isolation systems." Earthquake Engineering & Structural Dynamics, Vol. 46(14), 2017, pp.2337-2353.

[9] FURINGHETTI, M., PAVESE, A., QUAGLINI, V., DUBINI, P. "Experimental investigation of the cyclic response of double curved surface sliders subjected to radial and bidirectional sliding motions." Soil Dynamics and Earthquake Engineering, Vol. 117, 2019 pp. 190-202.

[10] GANDELLI, E., QUAGLINI, V. "Effect of the static coefficient of friction of curved surface sliders on the response of an isolated building". Journal of Earthquake Engineering, 2018, 1-29.

[11] KITAYAMA, S., & CONSTANTINOU, M.C. "Effect of displacement restraint on the collapse performance of seismically isolated buildings." Bulletin of Earthquake Engineering, 1-20, 2019.

[12] KITAYAMA S, CONSTANTINOU MC, "Collapse performance of seismically isolated buildings designed by the procedures of ASCE/SEI 7". Eng Struct 164:243–258, 2018.

[13] American Society of Civil Engineers. "Minimum Design Loads for Buildings and Other Structures." ASCE/SEI 7-10. 2013.

[14] FEMA, P. 695 (2009). "Quantification of building seismic performance factors." 2001

[15] https://www.fipmec.it

[16] STRUCTURAL ENGINEERS ASSOCIATION OF CALIFORNIA. SEAOC structural/seismic design manual. Volume 5: Examples for seismically isolated buildings and buildings with supplemental damping. Published January 2014.

[17] PRE-STANDARD, F. E. M. A. commentary for the seismic rehabilitation of buildings, report FEMA-356. Washington, DC: SAC Joint Venture for the Federal Emergency Management Agency, 2000.

[18] MCKENNA, F., FENVES, GL., SCOTT, MH., JEREMIC, B., "Open system for earthquake engineering simulation (OpenSEES)." Berkeley (CA): Pacific Earthquake Engineering Research Center, University of California, 2000.

[19] OpenSEES (2006). Open System for Earthquake Engineering Simulation, *Pacific Earthquake Engineering Research Center*, University of California, Berkeley, Available at http://opensees.berkeley.edu/.

[20] Constantinou, M.C., Mokha, A., Reinhorn, A. (1990). Teflon bearings in base isolation. II: modeling. *Journal of Earthquake Engineering*, 116(2):455–474.

[21] BARONE, S., CALVI, G.M., PAVESE, A. "Experimental dynamic response of spherical friction based isolation devices," Journal of Earthquake Engineering. Vol 23- Issue 9, 2019.

[22] RAGNI, L., CARDONE, D., CONTE, N., DALL'ASTA, A., Di CESARE, A., FLORA, A., LECCESE, G., MICOZZI, F., PONZO, F.C. "Modelling and seismic response analysis of Italian code-conforming base-isolated buildings." Journal of Earthquake Engineering. Vol. 22, 2018 pp. 198-230.

[23] DI CESARE A., PONZO F.C., TELESCA A., NIGRO D., CASTELLANO M.G., INFANTI S., FICHERA S., BIONDI B. "Modelling of the over stroke displacement of Curved Surface Sliders using OpenSEES". First Eurasian Conference on OpenSEES, Hong Kong, 20-21 June 2019.

[24] IERVOLINO, I., SPILLATURA, A. BAZZURRO, P. [2018] "Seismic structural reliability of code-conforming Italian buildings," Journal of Earthquake Engineering. Vol. 22, 2018 pp. 54-73.

[25] BAKER, Jack W. "Efficient analytical fragility function fitting using dynamic structural analysis". Earthquake Spectra, 2015, 31.1: 579-599.